

VICTORIA UNIVERSITY
MELBOURNE AUSTRALIA

Measurements of specific heat capacity of common building materials at elevated temperatures: a comparison of DSC and HDA

This is the Accepted version of the following publication

Pooley, Lachlan, Abu-Bakar, Ariza Sharikin, Cran, Marlene, Wadhwani, Rahul and Moinuddin, Khalid (2019) Measurements of specific heat capacity of common building materials at elevated temperatures: a comparison of DSC and HDA. *Journal of Thermal Analysis and Calorimetry*. ISSN 1388-6150

The publisher's official version can be found at
<https://link.springer.com/article/10.1007%2Fs10973-019-09124-5>
Note that access to this version may require subscription.

Downloaded from VU Research Repository <https://vuir.vu.edu.au/40174/>

Measurements of specific heat capacity of common building materials at elevated temperatures - A comparison of DSC and HDA

Lachlan I. Pooley¹, Ariza S. Abu-Bakar², Marlene J. Cran¹, Rahul Wadhwani¹, Khalid A. M. Moinuddin^{1*}

¹Institute for Sustainable Industries and Liveable Cities, Victoria University, PO Box 14428, Melbourne, Victoria 8001, Australia;

²School of Housing, Building and Planning, Universiti Sains Malaysia, 11800. Penang, Malaysia;

*Corresponding author: khalid.moinuddin@vu.edu.au; Tel.: +61 3 9919 8042

Abstract

The objective of this study is to investigate how the specific heat capacity (c_p) value of a material changes with respect to temperature and heating rate of that material. In-depth knowledge in the variation of c_p will provide a better knowledge of the thermo-physical properties of these materials and will increase the capabilities and fidelity of computational fluid dynamics (CFD) based fire modelling. The models and simulations are reliant on input data gained through experimentation and this allows for the present study to provide such input data and trends, which are useful in understanding how fires respond in different situations. The value of c_p in relation to the rate of temperature change has been measured using differential scanning calorimetry (DSC) and hot disk analysis (HDA). This study encapsulates the determination of c_p values, trends and equations for poly(methyl methacrylate (PMMA), pinewood, pinewood char and two fabrics: cotton and wool. The c_p values were found to increase with the sample temperature and for two fabrics, they vary with the change in heating rate. The derived equations show that c_p values from DSC and HDA are comparable. To include these relationships in CFD-based fire models, a set of suggestions have been made.

Keywords: DSC; hot disk analyser; specific heat capacity; PMMA; pinewood; fabric

Nomenclature:

β_s Heating rate, K min⁻¹

C Specific heat, J g⁻¹ K⁻¹

c_p Specific heat capacity, J g⁻¹ K⁻¹

$c_{p,a}$ Specific heat capacity, J g⁻¹ K⁻¹

c_r Specific heat capacity of reference sample, J g⁻¹ K⁻¹

$\frac{dH}{dt}$ Heat flow to the sample, mW

$\frac{dH_r}{dt}$ Heat flow to the reference material, mW

H Enthalpy, J

m Mass, g

m_o Sample mass, g

40	m_r	Reference mass, g
41	p	Pressure constant
42	Q	Heat flow, J
43	ΔQ	Change in heat flow, mW
44	T	Temperature, °C or K
45	ΔT	Change in temperature, °C or K

46 1 Introduction

47 Fire models and simulations are much more cost effective in determining important factors that contribute
 48 to fire behaviour, prevention, suppression and control. Full and medium-scale experimentation in compartment
 49 fire testing, however, is cost prohibitive. This constraint therefore requires the use of numerical fire modelling
 50 which needs input parameters from a controlled miniature and/or bench-scale testing environment to gather
 51 fundamental experimental data. It is imperative that the data from experimental testing and analysis are able to
 52 validate models of fire behaviour [1]. More accurate predictions of fire can lead to a better understanding of the
 53 associated fire risk and reliable fire prevention and systems can be implemented to reduce the risk. This is
 54 economically beneficial for insurers, building owners and clients, who would benefit from a reduction in fire
 55 damage subsequently reducing the cost of a fire incidence.

56 Poly(methyl methacrylate (PMMA), pinewood, cotton and wool are some common materials that are used
 57 throughout the building and manufacturing industry. These materials have a wide range of uses and are found
 58 in diverse environments in which they are typically clustered. In instances where these materials are exposed to
 59 a fire situation, the surrounding temperature varies as the fire grows or declines and the materials can be heated
 60 with different heating rates. With regard to the heating rate of the material, the accurate measurement of specific
 61 heat capacity (c_p), among other thermo-physical and flammability parameters, is required for input values for
 62 computational fluid dynamics (CFD) based fire models such as fire dynamic simulation (FDS) [2] to improve
 63 fidelity. A variation in heating rate is known to have an effect on the thermo-physical properties of different
 64 materials [3, 4] and c_p has an influence on many thermo-physical processes that occur during a fire including
 65 ignition point, phase change and chemical interactions during pyrolysis. The c_p value is useful when determining
 66 regions of thermal activation, volatilization and pyrolysis, therefore, studies are needed to focus on estimating
 67 c_p of the materials. In CFD based fire simulations, it is crucial that accurate input values are used including
 68 variations in terms of temperature, heating rate, heat flux etc. [5]. Small scale testing can be used to accurately
 69 determine the c_p value of the materials as a prerequisite for simulation but also to verify if these simulations are
 70 predictive of large fires [6].

71 The c_p value can be determined using numerous methods with varying degrees of accuracy and sources of
 72 errors with different calorimetry instruments [7] including the differential scanning calorimeter (DSC) and hot
 73 disk analyser (HDA) apparatus. These instruments can provide a range of thermo-physical data for a wide range
 74 of materials and are readily commercially available. The DSC can provide quantitative and qualitative data on
 75 transitions of materials with temperature, heating rate, degradation environment, and can be used to estimate
 76 c_p , thermal conductivity (k), latent heat, transition temperature and enthalpy [4, 7]. However, the DSC requires
 77 significant effort in post-processing the raw data to obtain c_p and k values. Moreover, the thermal behaviour of
 78 the material studied is normally compared with a reference material such as sapphire making the process time
 79 consuming and expensive. The HDA instrument can be used to determine the thermal diffusivity, k and c_p and
 80 its companion software provides these values readily. The primary variance between the two instruments is that
 81 the DSC gives c_p as a function of both heating rate and temperature, whereas the HDA provides the data as a

function of temperature only. Differential thermal analysis (DTA) is another technique closely related to the DSC, however, the DSC can provide greater accuracy and is the preferred method of determining c_p [8]. Although literature exists on the effect of temperature on PMMA and various species of pinewood, there are few reports of the effect of heating rate on pinewood char, cotton and wool [9]. Goodrich [9] observed that there are substantial difficulties with materials of a similar nature to cotton and wool which may account for the lack of conclusive research in this particular area.

For some materials, especially those undergoing endothermic reactions, heating rates higher than 5 K min^{-1} are recommended for thermal analysis [10] and are considered to be macroscopic heating rates. Therefore, in the present study, c_p was measured as a function of the rate of temperature change for heating rates of 50, 100 and 200 K min^{-1} with these high heating rates likely to occur in building fires. Using DSC measurements, raw data was obtained using the sapphire method [11] and c_p was calculated using post processing in MATLAB. Using the same materials, experiments using HDA equipment were performed where the sample was heated in an oven until a thermocouple attached to the sample showed that it reached the desired temperature then the c_p value was measured at that temperature. The data from both sets of apparatus was used to develop possible equations for use in fire engineering applications and also within fire modelling algorithms.

2 Materials and Methods

2.1 Concept of Specific Heat Capacity for Determination for using DSC

c_p is the amount of thermal energy (J) that is required to change the temperature of 1 g of material by 1 K at constant pressure and expressed in $\text{J g}^{-1} \text{ K}^{-1}$. Thermodynamically, c_p is determined by the equation:

$$c_p = \left(\frac{\partial H}{\partial T} \right)_p \quad (1)$$

where, H is enthalpy; T is temperature of the system; p is the pressure constant.

The derivation of c_p can also be expressed as:

$$c_p = \frac{\delta Q}{dT} \cdot \frac{1}{m} \quad (2)$$

where, Q is heat; m is mass. The amount of energy or heat that is exchanged for the change in temperature from T_1 to T_2 for a given mass m and specific heat $c_p(T)$.

$$Q = m \int_{T_1}^{T_2} c_p(T) dt \quad (3)$$

The characteristic equation that is used to determine the c_p from DSC is:

$$c_p = \frac{\Delta Q}{\Delta T} \quad (4)$$

Equation (4) can be utilised using the DSC curves of the heat flow and physical quantity.

Taking into account the heating rate, c_p can be calculated using the following formula:

$$c_p = \frac{1}{m_o \cdot \beta_s} \cdot \frac{dH}{dt} \quad (5)$$

where β_s is the heating rate of the sample; m_o is the sample mass; $\frac{dH}{dt}$ is the blank curve corrected heat flow to the sample. The sample is required to be stable throughout the heating range in order to determine the specific heat.

Depending on the method used to determine c_p , if a sample or known reference material is used then c_p is calculated by:

$$c_p = \frac{m_r}{m_o} \cdot \frac{dH/dt}{dH_r/dt} \cdot c_r \quad (6)$$

where m_r is the reference mass; c_r is the specific heat capacity of the reference mass; $\frac{dH_r}{dt}$ is the heat flow of the reference. The temperature range for this study was selected up to which no thermal degradation (mass loss) occurs in order to avoid a mass correction for the evaluation of the c_p . Thermogravimetric analysis data from a previous study [12] and a concurrent study [13] show that PMMA, pine and cotton have minimal mass loss up to 300 °C and for wool up to 275 °C. Therefore, only results up to these regions are evaluated.

The concept, and experimental technique to obtain HDA data can be found in [5, 12]. It should be noted that HDA does not require calibration since the Krapton sensor infused with nickel wire is calibrated by the manufacturer. The data affected by the contact sensor resistance lies in the non-linear region at the start of the experiment and is thus automatically removed from the calculation of material properties [14]. The following sections describe the DSC method for obtaining the c_p .

2.2 Obtaining c_p using DSC

2.2.1 Sample Preparation

The samples of PMMA were crushed into small granules approximately 1 mm² or smaller. Pinewood dust and parings of approximately 0.6-1 mm² were used. The cotton and wool samples were cut into small fragments ranging between 0.5 and 1.2 mm². Sample masses between 1.3 and 4.2 mg were used to ensure that the DSC could obtain a suitable measurement signal. The sample weights also ensured the crucibles were not over filled which potentially could have hindered the measurement of heat flow. Aluminium crucibles of 40 µL capacity were used in a Mettler Toledo DSC instrument [15]. Weighing errors were minimised with the use of a microbalance. Additionally, samples were reweighed when consistency between samples varied. The samples were placed in a conditioning unit prior to being encapsulated in the crucibles to reduce the moisture content in the materials, and also to verify the affect that moisture content has on materials when determining c_p . The relative humidity of the conditioning unit where the samples were kept was approximately 50% at 23°C.

2.2.2 Experimental/operating procedure

The DSC instrument was fully calibrated by the indium standard prior to sample measurements [16]. During the measurement, an inert atmosphere was created under a nitrogen flow of 50 mL min⁻¹. This represents an atmosphere in the absence of air which occurs when during flaming combustion thus preventing air reaching the burning material. The sapphire method for c_p determination was used as this method produces an accuracy that is within ± 2% [10, 12]. This method has been experimentally noted to have a variation of ± 5% for the value of sapphire material [17].

A “baseline” or blank measurement was performed for each heating rate (50, 100 and 200 K min⁻¹) in order to determine the signal bias in the system. This was obtained by determining the response of both crucibles when empty and allows for the signal bias to be removed from the data. A reference test for each heating rate was performed to ascertain the difference between the sapphire reference material with well-defined known specific heat values and the experimental sample. All of the results obtained were blank curve corrected and performed in triplicate.

There are two predominant methods of sealing the sample crucibles, namely without lid pinholes [4, 18], and with pinhole pierced lids [19]. Rath et al. [20] compared the used of an open pan and one with a lid pinhole and found that the presence of the lid effected both the heat flow and exothermic thermal effect of the sample. Other studies have also shown the effect of heat rate on samples and also the uncertainty of the results from DSC [21, 4, 22]. From these studies, it appears that the pinhole lid has a minimal effect depending on whether

gasses are released from the sample during the heating process. The test material and the reference were placed into individual aluminium crucibles which were then sealed with pierced lids. The data from the DSC was recorded, then analysed using MATLAB in order to obtain the c_p from the data. Taking into account the uncertainty of sample mass, variations between samples and DSC accuracy [21, 23], the standard error was estimated to be $\pm 3\text{-}5\%$.

3 Results and Discussion

With all four materials, we either observe moisture evaporation or phase transition (such as melting) or both. Such physical phenomenon involves enthalpy changes which are not part of the specific heat capacity. In literature [24] a combination of the specific heat capacity and additional enthalpy changes are describes as "apparent specific heat capacity" and we use $c_{p,a}$ as the symbol of it. We have plotted "apparent specific heat capacity" in Figures 1-7. However, the equations of c_p were determined from data and trends of the experimental data excluding enthalpy changes. The equation type has been selected for fire engineering purposes and CFD-based fire modelling simulations. Fire engineering has been emphasized over computer simulations, as fire engineers are more reliant on desktop computational methods since they typically do not have access to extensive experimental data resources and simulation computation. This has therefore limited the calculations to linear and polynomial equations.

3.1 PMMA

Figure 1 shows the $c_{p,a}$ of PMMA tested between 25 and 300 °C at different heating rates between 50 and 200 K min⁻¹. However, the data below 70 °C for 200 K min⁻¹ and 45 °C for 100 K min⁻¹ are excluded due to uncertainty in the initial measurement.

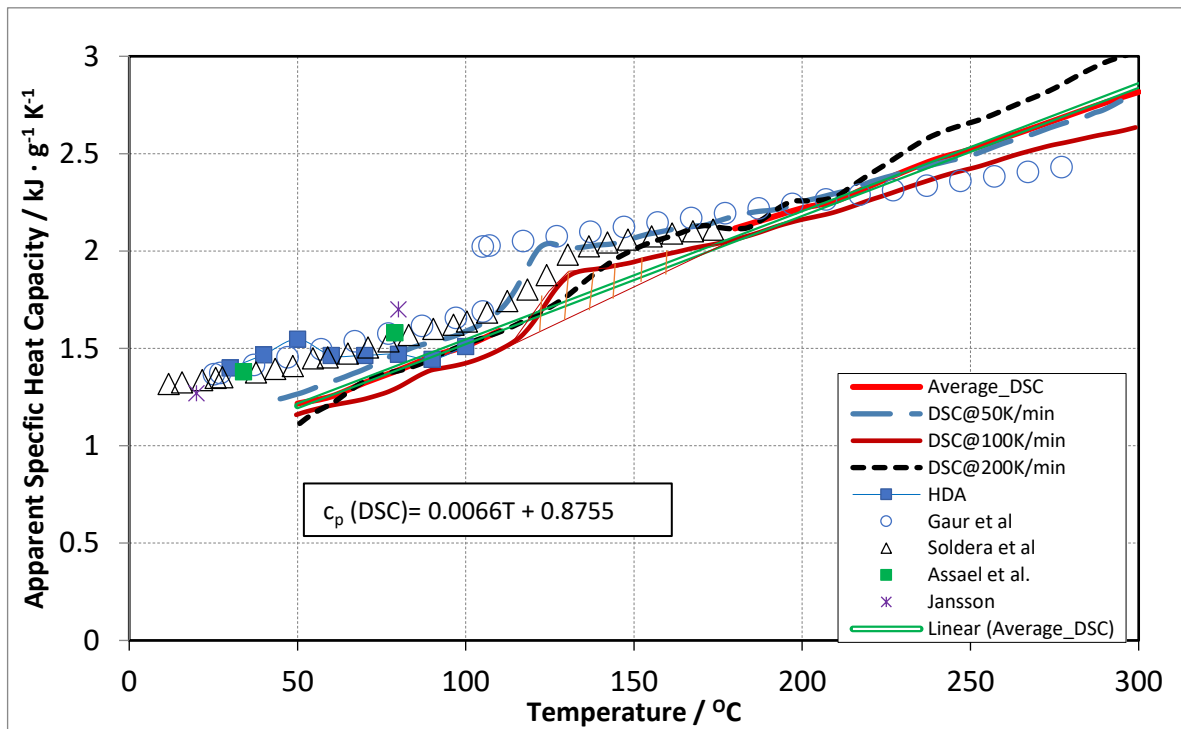


Figure 1. Apparent specific heat capacity variance of PMMA. The hatched pattern shows exemplar phase transition enthalpy as well as the difference between the specific heat capacity and the apparent specific heat capacity.

It can be observed that between 120 °C and 145 °C there is a peak in all $c_{p,a}$ - temperature profiles which is an indication of transition from a solid state to a melted state. As an example, phase transition enthalpy for 100 K.min⁻¹ profile is shown as hatched pattern and this shows the difference between the specific heat capacity and the apparent specific heat capacity. This transition was also observed by Gaur et al. [25] and Soldera et al. [26] as shown in Figure 1. For this reason, the c_p values are obtained using HDA up to 100 °C as the equipment is only designed to obtain the data from a solid state where no phase change of material or significant degradation of material takes place. The c_p values from HDA are also plotted in Figure 1 and the data between two apparatus are markedly comparable. The c_p values from the DSC (excluding phase transition range) have been averaged as the heating rates ranged from 50 to 200 K min⁻¹ and the averaged profile is presented in Figure 1. Undertaking a least squares analysis, we obtain a relationship presented as Eq (7), where T is in °C:

$$c_p \text{ (DSC)} = 0.0066 T + 0.8755 \text{ kJ g}^{-1} \text{ K}^{-1} \text{ (r}^2=1.0) \quad (7)$$

This equation follows the c_p profile obtained for 200 K min⁻¹ prior to melting, after melting the equation follows the c_p profile obtained for 50 K min⁻¹. Both HDA data and Eq (7) (averaged c_p from DSC) are compared with other literature studies. Data from Assael et al. [27] and Jansson [28] show linear relationships and their values are close to the values obtained in the current study. Prior to and after melting, linear relationships are also observed by Gaur et al. [25] and Soldera et al. [26]. Overall literature values are close to those in the current study.

3.2 Pinewood: Virgin and Char

Figure 2 and Figure 3 show the $c_{p,a}$ values of virgin pinewood. A peak bordering 100°C in the HDA data represents a moisture affected region with similar peaks more pronounced in the DSC data. At lower heating rates, the peaks are higher although they occur over a smaller temperature range. As the water evaporates at 100 °C, we can assume that these regions are affected by moisture content and its evaporation. Figure 2 shows this region affected by evaporation which ends between 170 °C at a heating rate of 50 K min⁻¹ (moisture evaporation enthalpy is shown by hatched pattern) and 217 °C at a heating rate of 200 K min⁻¹ for the data obtained using the DSC. Above these temperatures, the c_p value increases with temperature.

In Figure 3, data beyond the moisture affected region is represented up to 300 °C. The c_p value changes with the rate of heating are apparent within one thermal set, comprising data of 50 to 200 K min⁻¹. The values in 100 and 200 K min⁻¹ are close to each other in relative terms and the values of 50 K min⁻¹ are higher which may be due to the effect of thermal transport. The sudden drop at 240 °C for the data obtained at 50 K min⁻¹ can be attributed to pressure from vapour being released from the timber causing the seal and pinhole on the crucible lid to widen. This sudden endothermic peak in the data accounts for the shape of the graph.

In Figure 3, literature data [29-32] from dry wood is also presented although it should be noted that Gupta et al. [29] used a DSC to measure the c_p at 5 K min⁻¹ heating rate. Moreover, the literature data [29-31] is only reported up to 140 °C, whereas the current study values are extended to 300 °C. From 160 to 300 °C, the c_p values from the DSC have been averaged (without endothermic data) with the profile presented in Figure 3 and a relationship presented as Eq (8) is obtained undertaking a least squares analysis, where T is in °C:

$$c_p \text{ (DSC)} = 0.004 T + 0.6554 \text{ kJ g}^{-1} \text{ K}^{-1} \text{ (r}^2=0.94) \quad (8)$$

Eq (9) can be derived from the HDA data (excluding the data within the moisture affected region) [5], where T is in °C:

$$c_p \text{ (HDA)} = -10^{-5} + 0.0057 T + 0.9904 \text{ kJ g}^{-1} \text{ K}^{-1} \text{ (r}^2=0.98) \quad (9)$$

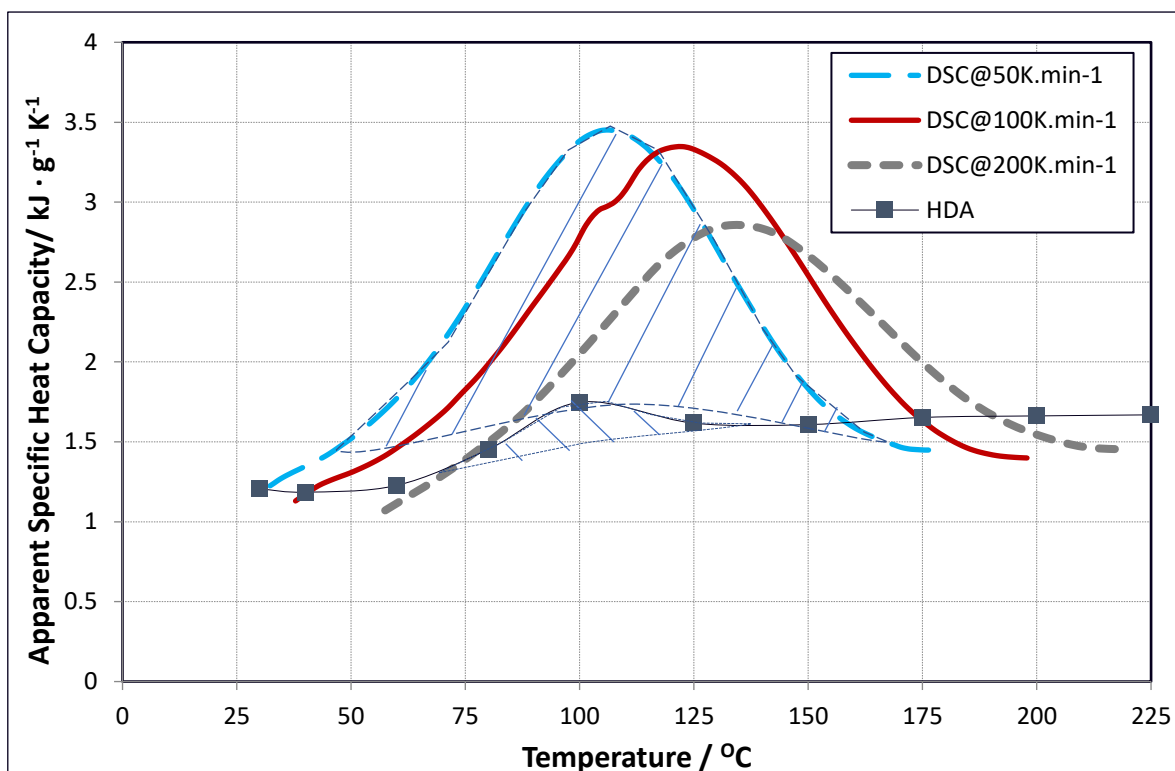


Figure 2. Apparent specific heat capacity variance of pinewood (moisture influenced region). The hatched pattern shows exemplar moisture evaporation enthalpy.

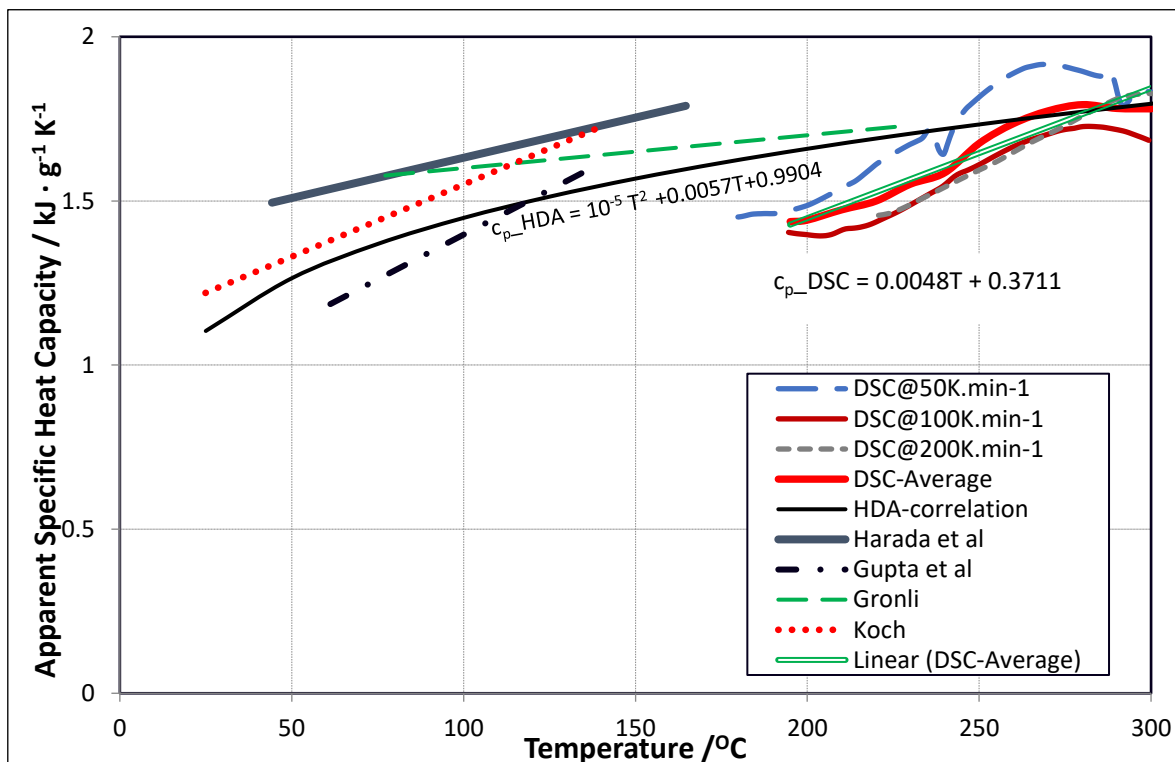


Figure 3. Apparent specific heat capacity without moisture evaporation region of pinewood

212 The DSC data could not be compared with the literature data since up to 170°C, the data is moisture
 213 affected. Yet, the HDA appears to be comparable with the literature data giving us confidence in our
 214 experimental procedure. Literature values show similar trends that conform to the current data given different

species of timber. They show the values at lower temperature ranges that are not affected by the moisture evaporation region and can be attributed to using completely dry wood for experiments. It should be noted that a diverse range of timbers exist and that even variation exists within the same species of timber.

Figure 4 shows the $c_{p,a}$ of pinewood char tested where the samples were superfluous from larger scale testing. The time taken between testing allowed moisture to penetrate the samples by the time DSC tests were conducted and this is observed in the results obtained. The enthalpy change in the moisture affected region can be observed in Figure 4 for the DSC experiments. Moisture evaporation enthalpy for 50 K.min⁻¹ profile, as an example, is shown as hatched pattern which can be considered the difference between the specific heat capacity and the apparent specific heat capacity. Since the HDA data is not affected by moisture, this data shows an overall increase in c_p with increasing temperature with the data from either side of the moisture region presented in Figure 4.

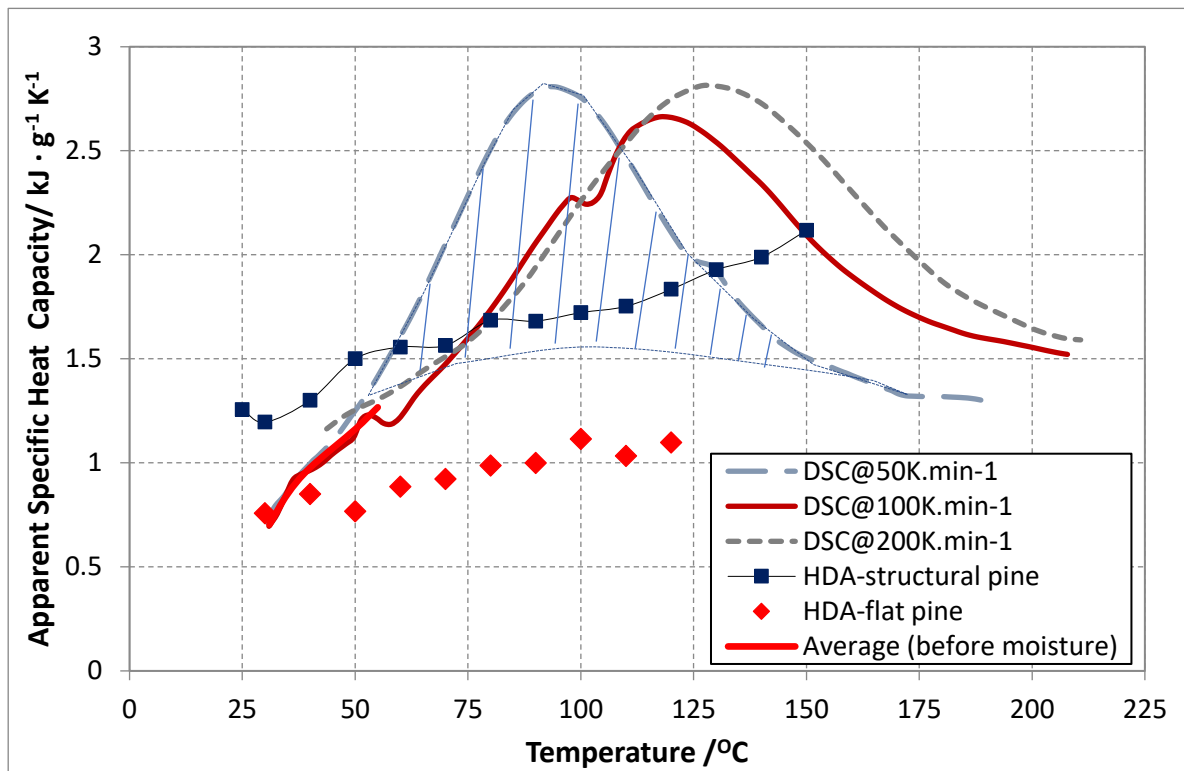


Figure 4. Variation of $c_{p,a}$ (DSC data) and c_p (HDA data) with temperature for pine char. The hatched pattern shows exemplar moisture evaporation enthalpy.

Increasing linear relationships with temperature proposed by Gupta et al. [29], Gronli et al. [31] and Koufopoulos et al. [33] are presented in Figure 5 along with the current study data (moisture affected DSC data are excluded). At the lower end of the temperature range, the data from the aforementioned studies show values that are comparable to the HDA data of flat-pine char obtained is more aligned with the literature data. From the HDA data, Eq (10-11) was derived [5], where T is in °C:

$$\text{Structural pine } c_p \text{ (HDA)} = 0.00655 T + 1.0897 \text{ kJ g}^{-1} \text{ K}^{-1} \text{ (} r^2=0.96 \text{)} \quad (10)$$

$$\text{Flat pine } c_p \text{ (HDA)} = 0.00394 T + 0.6456 \text{ kJ g}^{-1} \text{ K}^{-1} \text{ (} r^2=0.83 \text{)} \quad (11)$$

The DSC data shows that between 50 and 200 K min⁻¹, the effect of heating rate (thermal transport) on c_p is not significant. The empirical relations that were observed between temperature and c_p outside the area affected by moisture evaporation is presented in Figure 5 with Eq (12) determined:

$$c_p = 0.0028 T + 0.8587 \text{ kJ g}^{-1} \text{ K}^{-1} (r^2=0.88) \quad (12)$$

Extrapolation of the data obtained by Koufopoulos et al. [33] and Gupta et al. [29] shows consistency with the DSC data of the present study. In this case, the data of Koufopoulos et al. [33] runs almost equivalent with Eq (12).

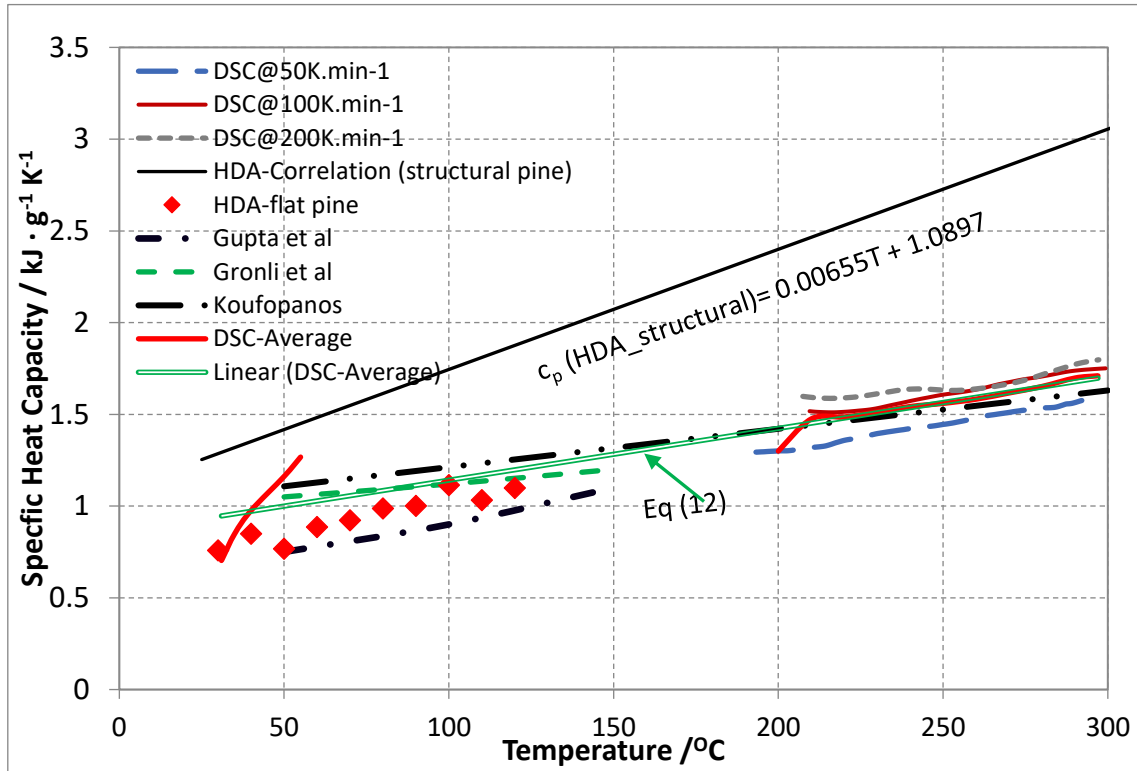


Figure 5. Variation in c_p for pinewood char excluding the moisture affected region

3.3 Cotton and Wool Fabrics

Figure 6 shows variation in the $c_{p,a}$ for cotton and similar to pinewood, the moisture content results in enthalpy change in the vicinity of 100°C. The region of moisture evaporation can be observed in Figure 6, though this is a subtle representation. The sudden spike in c_p values observed at around 260 °C for all heating rates can be attributed to the phase transition occurring in the cellulose structures within the cotton [34]. In all cases this is a significant but not unexpected spike since the cellulose content of cotton is around 90% [35]. As an example, moisture evaporation and phase transition enthalpy for 50 K.min⁻¹ profile are shown as hatched patterns and these show the difference between the specific heat capacity and the apparent specific heat capacity.

The HDA data is also plotted in Figure 6 and a steadily increasing trend in the c_p is observed after the moisture evaporation region (hatched pattern) was removed. The HDA data generally conforms to the same characteristic trend present for the DSC with c_p values that are comparable. Literature value for cotton from Harris [36] at lower temperature is presented in Figure 6 which falls slightly above the range of the DSC values, but below HDA, for values at the lowest temperatures presented.

To obtain a quantitative trend, the data related to the moisture evaporation and phase transition regions were removed. Then, from 40 to 290 °C, the c_p values from the DSC have been averaged for the heating rates

50 to 200 K min⁻¹. It can be observed the c_p –temperature profiles from these three heating rates are close to each other implying that the effect of thermal transport is not significant. This averaged profile is also presented in Figure 6 and Eq (13) [where T is in °C] was obtained by a least square's regression analysis:

$$c_p (\text{DSC}) = 0.0052 T + 0.9255 \text{ kJ g}^{-1} \text{ K}^{-1} (r^2=0.99) \quad (13)$$

Similarly, Eq (14) was derived from the HDA data [5] where T is in °C:

$$c_p (\text{HDA}) = 0.0024 T + 1.6238 \text{ kJ g}^{-1} \text{ K}^{-1} (r^2=0.78) \quad (14)$$

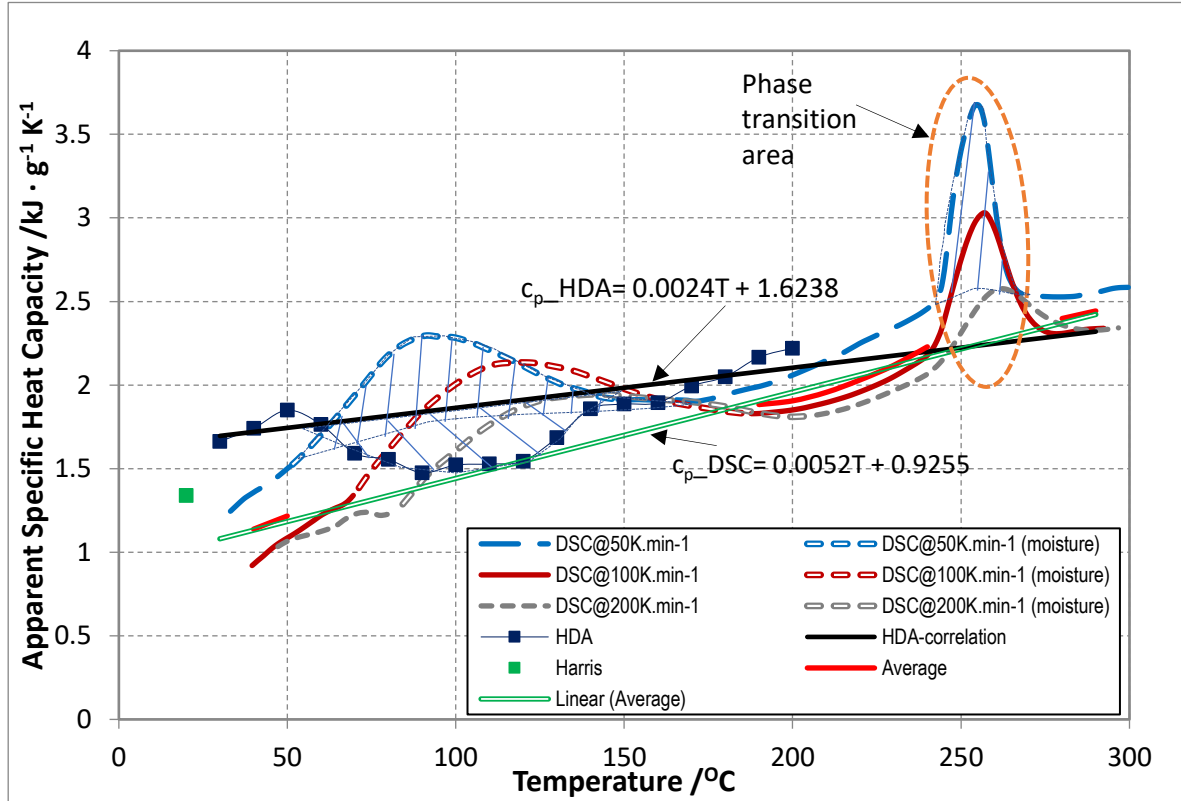


Figure 6. Variation of apparent specific heat capacity for cotton. The hatched pattern shows exemplar moisture evaporation and phase transition enthalpy as well as the difference between the specific heat capacity and the apparent specific heat capacity.

Figure 7 shows the variation of $c_{p,a}$ for wool tested using both the DSC and HDA apparatus, though HDA experiments were not conducted beyond 200 °C. Wool is affected by moisture evaporation in the same manner as cotton and pinewood. Both the DSC and HDA data shows that shortly after the initiation of heating, the moisture affected region is apparent. Phase transition regions are observed in the DSC data which can be attributed to the decomposition within the fibres of wool or swelling decrystallisation of various types of amino acids present in wool [30, 31]. This can also contribute to the secondary peak and linear increase observed as the acids break down into base constituents above the temperature of 225 °C [37, 38]. Similar to cotton data presentation in Figure 6, the moisture evaporation and phase transition enthalpy for 50 K.min⁻¹ profile are shown as hatched patterns.

To obtain a quantitative trend, all DSC data were analysed excluding the moisture evaporation and phase transition. The DSC obtained c_p values were averaged over all three heating rates data in three regions: (i) from 25 to 68 °C, (ii) from 180 to 240 °C, and (iii) from 260 to 275 °C. Undertaking a least squares analysis of the average profile, the relationship obtained is presented in Eq (15) for the DSC data and in Eq (16) for the HDA data [5], where T is in °C:

$$c_p (\text{DSC}) = 9 \times 10^{-7} \times T^3 - 0.000355 T^2 + 0.04237 T - 0.06137 \text{ kJ g}^{-1} \text{ K}^{-1} (r^2=0.94) \quad (15)$$

$$c_p (\text{HDA}) = 6 \times 10^{-5} \times T^2 - 0.0126 T + 1.85 \text{ kJ g}^{-1} \text{ K}^{-1} (r^2=0.91) \quad (16)$$

In general, the data from both test apparatus are comparable except at low temperatures. Figure 7 also presents a comparative literature value for sheep wool as reported by Tuzcu [39] which is slightly higher than the values from the current study although it should be noted that this literature data did not take into account temperature or heating rate. It can be observed that while the heating rate is varied, before and after the moisture evaporation region (until the phase transition occurs), c_p values differ considerably implying significant effect of thermal transport.

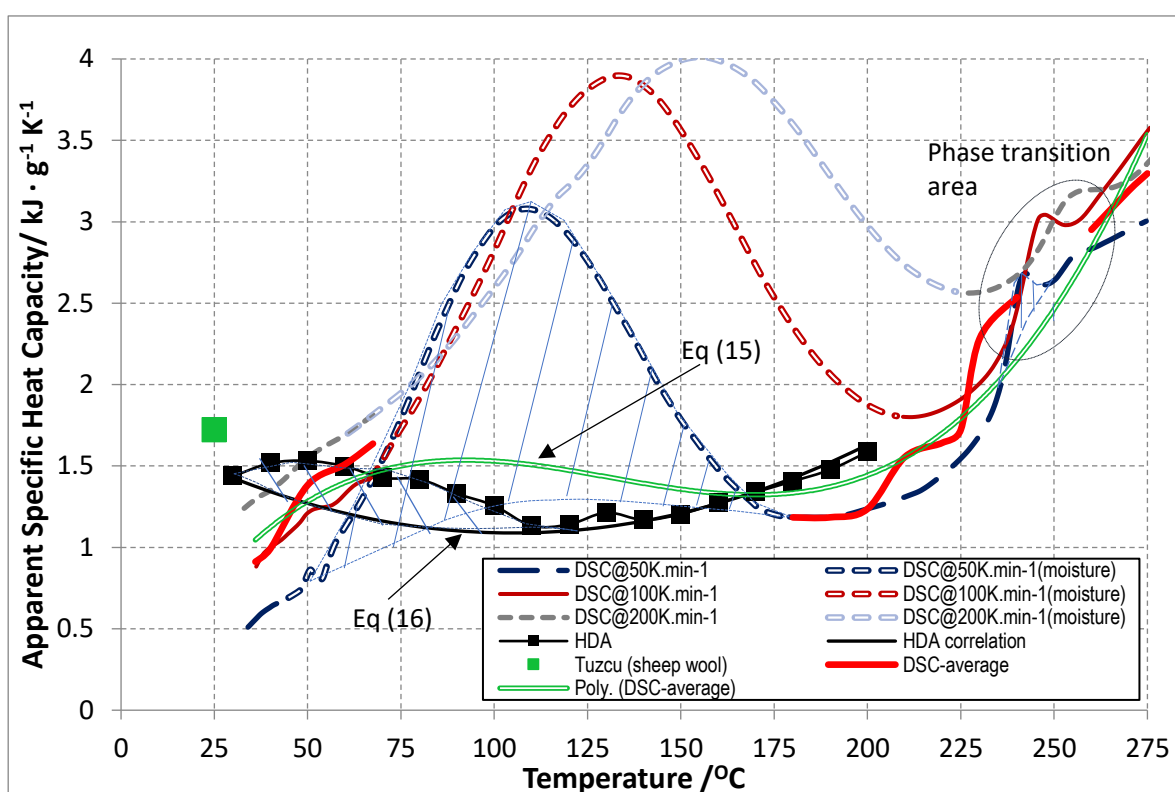


Figure 7. Variation of apparent specific heat capacity for wool. The hatched pattern shows exemplar moisture evaporation and phase transition enthalpy as well as the difference between the specific heat capacity and the apparent specific heat capacity.

A summary of the correlations developed for the tested materials is presented in Figure 8 and in general, it can be observed that as the temperature increases there is an increase in the c_p values. As shown, the difference between HDA and DSC measurements are not substantial. For each material, at a specific temperature, the values intersect and moving away from this intersection point, the difference increases. The maximum difference ranges for PMMA, pine, pine char, cotton and wool are ± 0.6 , ± 0.3 , ± 0.2 , ± 0.6 and $\pm 0.7 \text{ kJ kg}^{-1} \text{ K}^{-1}$. In the supplementary material, a method is recommended to enable the optimized use of the data.

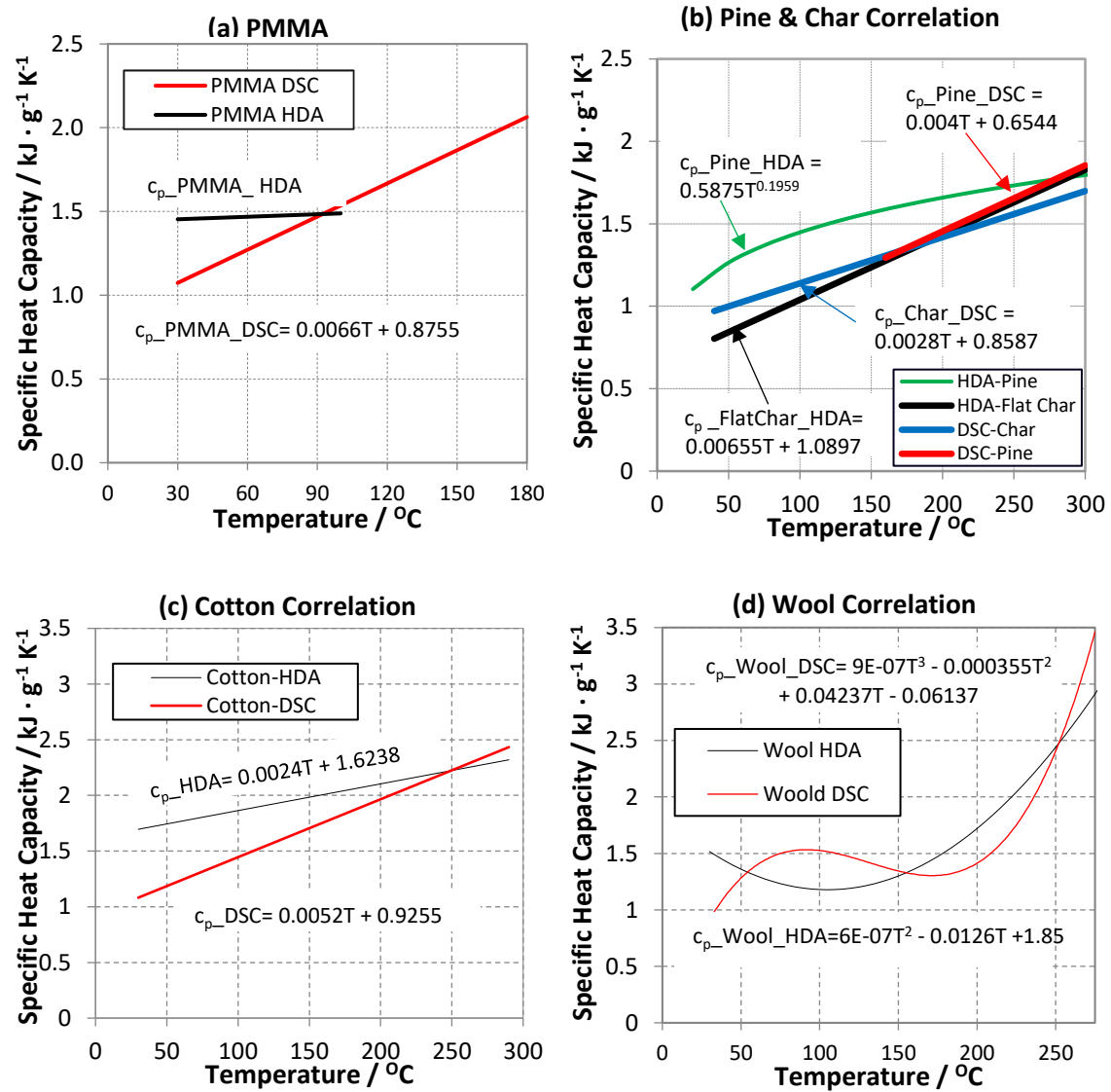


Figure 8. Correlations of c_p for (a) PMMA, (b) pinewood, virgin and char, (c) cotton, and (d) wool with temperature

4 Conclusions

The c_p values of common building materials tested with DSC and HDA apparatus are presented in this study with their trends determined with respect to temperature. The primary objective is to use the obtained c_p values in CFD-based fire simulations for fire engineering and research purposes. While the HDA measurement did not involve any heating rate, DSC measurements were conducted at heating rates of 50, 100 and 200 K min⁻¹ as these are likely to occur in substantial fires. DSC materials were roughly measured over a temperature range of 25 to 300 °C except for wool up to 275 °C. HDA measurements were conducted from 30 to 100 °C for PMMA, 30 to 225 °C pinewood, 25 to 150 °C for char and 30 to 200 °C for cotton and wool.

Of all the materials tested, PMMA was the only material not affected by moisture content and PMMA, cotton and wool all showed phase transitions at ~125 °C, ~260 °C and ~245 °C respectively. For similar materials, literature data was generally comparable to the data obtained in the current study data although typically at lower temperatures. This further supports the results obtained at higher temperatures and at different heating rate in the current study.

The DSC measurements of c_p values did not change significantly for PMMA and pine char between heating rates adopted in this study. For pine and cotton slight decrease as heating rate increased are observed. On the other hand, for wool c_p values considerably increased as heating rate increased. The effect of thermal transport varies due to chemical composition, physical and structural properties. It is also noted that the materials have different fibrous and cellulose structures.

Analysis of the DSC and HDA c_p values for the various materials studied enabled the development of empirical relationships. The relationships were developed from regions where phase changes were not occurring, and regions not affected by moisture evaporation. The relationships show that the difference between HDA and DSC are not substantial. These relationships can be used as input values for CFD-based fire simulations and models and all materials except for wool showed a linear increase of c_p values with increasing temperature. A second and third order curvilinear increase were observed for the c_p values with HDA and DSC measurement for wool. Some suggestions are made, in the supplementary material, for how to include these relationships in CFD-based fire models. The enhanced accuracy of the data will assist in providing higher fidelity simulations of fire scenarios which can be utilised in order to develop improved designs for reducing fire risk.

Funding:

This study was conducted through internal funding from Victoria University.

Conflicts of Interest:

The authors report no conflict of interest in this study.

References

1. Drysdale D. An introduction to fire dynamics. John Wiley & Sons; 2011.
2. McGrattan K, McDermott R, Weinschenk C, Overholt K, Hostikka S, Floyd J. Fire dynamics simulator (Sixth Edition) user's guide. Gaithersburg, Maryland, USA: National Institute of Standards and Technology; 2015.
3. Abu-Bakar A, Moinuddin K, editors. Effects of variation in heating rate, sample mass and nitrogen flow on chemical kinetics for pyrolysis. 18th Australasian fluid mechanics conference Launceston, Australia; 2012; Launceston, TAS.
4. Kousksou T, Jamil A, El Omari K, Zeraoui Y, Le Guer Y. Effect of heating rate and sample geometry on the apparent specific heat capacity: DSC applications. *Thermochimica acta*. 2011;519(1-2):59-64.
5. Abu-Bakar AS. Characterization of Fire Properties for Coupled Pyrolysis and Combustion Simulation and Their Optimised Use [PhD]. College of Engineering and Science: Victoria University; 2015.
6. Linteris GT, Gewuerz L, McGrattan KB, Forney GP. Modeling solid sample burning with FDS. National Institute of Standards and Technology, NISTIR. 2004;7178:36.
7. Czichos H, Saito T, Smith LE. Springer Handbook of Materials Measurement Methods. Springer Science+Business Media; 2007.
8. Mettler-Toledo. Heat capacity determination at high temperatures by TGA/DSC Part 1: DSC standard procedures. Schwerzenbach, Switzerland; 2010.
9. Goodrich TW. Thermophysical properties and microstructural changes of composite materials at elevated temperature: Virginia Tech; 2009.

10. Kodur VKR, Harmathy TZ. Properties of Building Materials. In: DiNenno PJ, Drysdale D, Beyler CL, Walton WD, Custer RLP, Hall JR, Jr. et al., editors. *SFPE Handbook of Fire Protection Engineering*. Third ed.: National Fire Protection Association; 2002. p. 155-81.
11. Hohne GWH, Hemminger WF, Flammersheim HJ. *Differential Scanning Calorimetry*. Springer-Verlag Berlin Heidelberg New York; 2003.
12. Abu Bakar AS, Cran M, Moinuddin KAM. Experimental investigation of effects of variation in heating rate, temperature and heat flux on fire properties of a non-charring polymer. *Journal of Thermal Analysis and Calorimetry*. 2019;137(2):447-59. doi:DOI: 10.1007/s10973-018-7941-0.
13. Abu Bakar AS, Cran M, Wadhwani R, Moinuddin KAM. Characterisation of pyrolysis and combustion parameters of charring materials most frequently found in buildings *Journal of Thermal Analysis and Calorimetry*. 2019;(in Press).
14. Thermtest I, inventor Thermtest Inc, assignee. *Hot Disk Thermal Constants Analyser Instruction Manual*. Canada 2012.
15. Mettler T, inventor DSC1 User's Manual. Switzerland 2011.
16. Mettler-Toledo. DSC Calibration, Temperature and Heat Flow. Mettler-Toledo, Switzerland. 2018. https://www.mt.com/au/en/home/supportive_content/matchar_apps/MatChar_HB805.html. Accessed 14 October 2018.
17. Shaw T, Carrol J. Application of baseline correction techniques to the “ratio method” of DSC specific heat determination. *International journal of thermophysics*. 1998;19(6):1671-80.
18. Milosavljevic I, Oja V, Suuberg EM. Thermal effects in cellulose pyrolysis: relationship to char formation processes. *Industrial & Engineering Chemistry Research*. 1996;35(3):653-62.
19. Shalaev EY, Steponkus PL. Correction of the sample weight in hermetically sealed DSC pans. *Thermochimica acta*. 2000;345(2):141-3.
20. Rath J, Wolffinger MG, Steiner G, Krammer G, Barontini FC, Cozzani V. Heat of Wood Pyrolysis. *Fuel*. 2003;82(1):81-91.
21. Rudtsch S. Uncertainty of heat capacity measurements with differential scanning calorimeters. *Thermochimica Acta*. 2002;382(1-2):17-25.
22. Strezov V, Patterson M, Zyma V, Fisher K, Evans TJ, Nelson PF. Fundamental aspects of biomass carbonisation. *Journal of analytical and applied pyrolysis*. 2007;79(1-2):91-100.
23. Dieck RH. *Measurement uncertainty: methods and applications*. ISA; 2007.
24. Höhne G, Hemminger WF, Flammersheim H-J. *Differential scanning calorimetry*. Springer Science & Business Media; 2013.
25. Gaur U, Lau Sf, Wunderlich BB, Wunderlich B. Heat capacity and other thermodynamic properties of linear macromolecules VI. Acrylic polymers. *Journal of Physical and Chemical Reference Data*. 1982;11(4):1065-89.
26. Soldera A, Metatla N, Beaudoin A, Said S, Grohens Y. Heat capacities of both PMMA stereomers: Comparison between atomistic simulation and experimental data. *Polymer*. 2010;51(9):2106-11.
27. Assael MJ, Botsios S, Gialou K, Metaxa IN. Thermal Conductivity of Polymethyl Methacrylate (PMMA) and Borosilicate Crown Glass BK7. *International Journal of Thermophysics*. 2005;26(5):1595-605. doi:10.1007/s10765-005-8106-5.
28. Jansson R. Measurement of thermal properties at elevated temperatures - Brandforsk Project 328-031. SP Report 2004:46; 2004.
29. Gupta M, Yang J, Roy C. Specific heat and thermal conductivity of softwood bark and softwood char particles☆. *Fuel*. 2003;82(8):919-27.

30. Harada T, Hata T, Ishihara S. Thermal constants of wood during the heating process measured with the laser flash method. *Journal of wood science*. 1998;44(6):425-31.
31. Gronli MG, Antal J, Varhegyi G. A Round-Robin Study of Cellulose Pyrolysis Kinetics by Thermogravimetry. *Industrial & Engineering Chemistry Research*, 38(6). 1999:2238–44.
32. Koch P. Specific heat of oven-dry spruce pine wood and bark. *Wood Science Vol 1* (4): 203-214. 1968.
33. Koufopoulos C, Lucchesi A, Maschio G. Kinetic modelling of the pyrolysis of biomass and biomass components. *The Canadian Journal of Chemical Engineering*. 1989;67(1):75-84.
34. Ayeni N, Adeniyi A, Abdullahi N, Bernard E, Ogunleye A. Thermogravimetric and kinetic study of methylolmelamine phosphate treated–cotton fabric. *Bayero Journal of Pure and Applied Sciences*. 2012;5(2):51–5.
35. Meilert K, Laub D, Kiwi J. Photocatalytic self-cleaning of modified cotton textiles by TiO₂ clusters attached by chemical spacers. *Journal of molecular catalysis A: chemical*. 2005;237(1-2):101-8.
36. Harris vM. *Handbook of Textile Fibers*. Harris Research Laboratories, Washington.; 1954.
37. Horrocks AR, Price D. *Fire Retardent Materials*. Abington Cambridge: Woodhead Publishing Limited; 2001.
38. Bras ML, Camino G, Bourbigot S, Delobel R. *Fire Retardancy of Polymers: The Use of Intumescence*. Cambridge: The Royal Society of Chemistry; 1998.
39. Tuzcu T. *Hygro-thermal properties of sheep wool insulation*: Delft University of Technology; 2007.